Spatial speckle characterization by Brownian motion analysis

Steve Guyot,* Marie-Cécile Péron, and Eric Deléchelle
Laboratory L.E.R.I.S.S, University Paris 12, 61 avenue du Général de Gaulle, 94010 Créteil, France
(Received 3 February 2003; revised manuscript received 1 June 2004; published 29 October 2004)

It is well known that the interactions between coherent monochromatic radiation and a scattering medium induce a speckle phenomenon. The spatial and temporal statistics of this speckle are employed to analyze many applications in laser imaging. The direct exposure of a photographic film, without a lens to the backscattered radiation, gives a speckle pattern. The main problem lies in the determination of those parameters which can efficiently characterize this pattern. In this paper, we present a fractal-theory-based stochastic approach to approximate the diffusion. In our opinion, this method is more appropriate for the classification of this nonlinear and nonstationary phenomenon than the classical frequency-based approach. The paper also presents several applications of this method which have employed for characterization of different test media.

DOI: 10.1103/PhysRevE.70.046618 PACS number(s): 42.30.Ms

I. INTRODUCTION

Speckle, which is an interference phenomenon, appears when a spatially coherent light interacts with a rough surface or propagates itself in a random medium. Such a phenomenon can be observed in many physical applications—e.g., microscopic images, stellar images, and others. There are two approaches of taking speckle into consideration. In one approach, speckle can be considered as a noisy phenomenon that pollutes observations. Hence the objective is to try to suppress it, as far as practicable. In another approach, one can consider that it contains a lot of information about the system under observation. The choice between these two points of view depends on the specific application—e.g., in our case, biomedical imagery. A systematic study of the statistical properties of the speckle was undertaken to investigate the classification of speckle in the context of particular dermatological pathologies. Figure 1 shows a speckle pattern produced by the laser illumination on a scattering medium. Its temporal and spatial characteristics depend on many factors; some of these are experimental factors—e.g., the wavelength, spectral bandwidth, or polarization of the illuminating radiation, which can be seen below. On the other hand, the characteristics of the speckle will also depend on some physical factors which are due to the properties of the observed media—e.g., texture, roughness, material, shape, and so on. As speckle is an interference and diffraction phenomenon, the frequency-based approach to study its behavior, through Fourier optics, is frequently undertaken [1–3]. Goldfischer [2] first investigated the statistical properties of the speckle employing the power spectral density and its autocorrelation function. The first- and second-order statistics of the speckle [4] allow many applications in imagery [5]. Many researchers have also explored the relationships between the speckle dimensions and the experimental conditions [6–8]. More recently, the utility of the third-order intensity correlations has been investigated for several different applications. For example, Genack and Drake [9] developed an expression for the correlation of two speckle fields at different frequencies and Webster *et al.* [10] successfully employed the third-order correlation to obtain the temporal response of a random medium.

In this paper, we present an original and general approach of the speckle pattern through the fractal theory. Our main research interest is to study the diffusion of light in human skin. In a spatial and dynamic study, the frequency-based approach cannot be a natural choice as the speckle observed is totally stochastic in nature. Hence a fractal-theory-based stochastic approach is presented in this paper, which can be efficiently employed in these situations. Using this approach, one can extract the parameters of the speckle texture—e.g., fractal dimension, statistical distribution of the grains of speckle, and multiscale correlation in the image. The present paper is organized as follows. In Sec. II, we detail the statistics of speckle that may be correlated with Brownian motion theory. Section III describes our fractal approach for the characterization of the speckle. Section IV is devoted to the presentation of the experimental setup, which has been employed in our laboratory to acquire the speckle. In Sec. V, a detailed description of the results achived by employing our method on test media consisting of solutions made of latex balls are presented. Finally, conclusions are presented in Sec. VI.

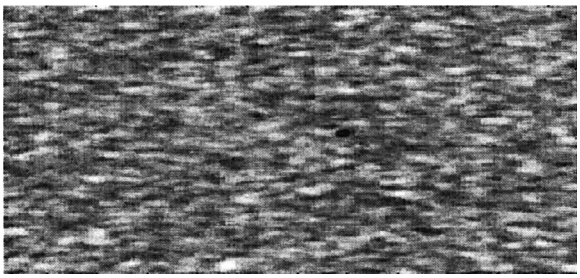

FIG. 1. The speckle pattern of a scattering medium.

*Electronic address: Guyot@univ-paris12.fr

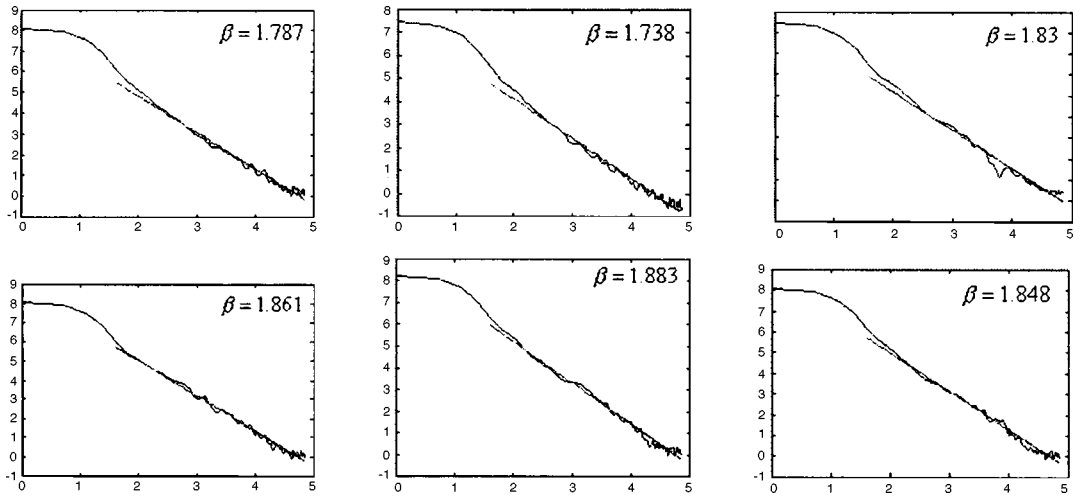

FIG. 2. Experimental spectral power densities (in logarithm) of the speckle patterns shown in Fig. 7 as a function of the logarithm of the frequencies (arbitrary unities).

II. STATISTICS OF THE SPECKLE AND THE CORRELATION WITH BROWNIAN MOTION THEORY

A. Amplitude, phase, and intensity statistics

Let us consider a monochromatic electric field (frequency ν_0)

$$U(x,y,z,t) = A(x,y,z)\exp(j2\pi\nu_0 t). \tag{1}$$

In the first-order statistics, the amplitude at one point in space is the sum of all out-of-phase contributions from many points of the scattering array. Hence, the amplitude can be given as

$$A(x,y,z) = \frac{1}{\sqrt{N}}\sum a_k(x,y,z) = \frac{1}{\sqrt{N}}\sum |a_k|\exp j\varphi_k. \tag{2}$$

As a result, the amplitude may be considered as a random walk in the complex plan.

Moreover, the following theoretical hypotheses should also be considered.

(i) The amplitude $a_k/\sqrt{N}$ and phase φ_k of the kth contribution are statistically independent and they are statistically independent compared to the others too.

(ii) The phases φ_k of the contributions are uniformaly distributed on $[0;2\pi]$.

Thus, from these hypotheses, Goodman [11] developed the probability density function [see Eq. (3)] for the real and imaginary parts of the field (employing the central limit theorem):

$$P(A^{(r)},A^{(i)}) = \frac{1}{2\pi\sigma^2}\exp\left\{-\frac{[A^{(r)}]^2+[A^{(i)}]^2}{2\sigma^2}\right\}, \tag{3}$$

with

$$\sigma^2 = \lim\inf\frac{1}{N}\sum\frac{\langle|a_k|^2\rangle}{2}. \tag{4}$$

So it is important to keep in mind that the amplitude conforms to a complex circular Gaussian statistic. Hence, the probability density function of the intensity in Eq. (5) can be expressed as

$$P(I) = \frac{1}{2\sigma^2}\exp\left(-\frac{I}{2\sigma^2}\right). \tag{5}$$

Equation (6) describes the behavior of the phase:

$$P(\theta) = \frac{1}{2\pi}. \tag{6}$$

It can be noted that there is an exponential decrease in the absolute intensity. Hence, the probability density function of the intensity detected by the camera is

$$P(I_d) = \left(\frac{n_0}{\langle I\rangle}\right)^{n_0}\frac{I_d^{n_0-1}}{\Gamma(n_0)}\exp\left(-\frac{n_0 I_d}{\langle I\rangle}\right). \tag{7}$$

Here n_0 may be interpreted as the number of speckle grains seen by the camera. Thus, this density evolves from an exponential of a Gaussian function when $n_0\to\infty$. The frequency-based approach is considered next.

B. Power spectral analysis

To keep this discussion concise, we only present the power spectral densities of several speckle patterns in Fig. 2. These results validate, partially, our approach based on Brownian motion theory. Some of the frequency-based approaches considered so far by researchers can be found in the literature [2,4]. It is very important to note that the speckles present a $1/f^{\beta}$ process for high frequencies. This type of a process is characteristic of an autosimilar process.

III. STOCHASTIC MODELING OF THE SPECKLE

For the sake of clarity, the model of one-dimensional Brownian motion is presented first and then it is extended to the two-dimensional case, for applications to speckle.

A. Brownian motion theory

Brownian motion (BM) is known as a Wiener process, observed for the first time by Brown in 1827. Brownian mo-

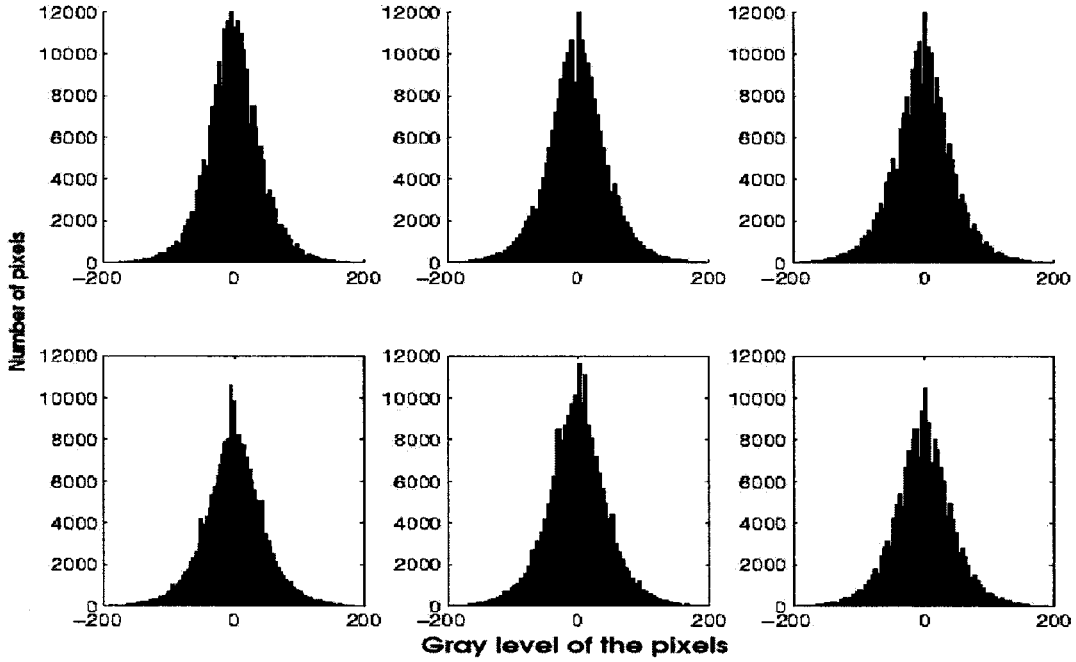

FIG. 3. Experimental distributions (for several values of Δr: 4, 8, 16, 32, 128, 256) of the intensity (speckle pattern showed in Fig. 1).

tion is a continuous but not derivable process, and its variance is proportional to the difference in time, as in Eq. (8) between t_1 and t_2:

$$\sigma^2 = \mathrm{Var}[X(t_2) - X(t_1)] \propto |t_2 - t_1|. \tag{8}$$

B. Generalization to fractional Brownian motion (FBM)

It is possible to generalize Brownian motion theory to all types of processes as expressed by Mandelbrot [12]. This extension has evolved from a previous statistical study by Hurst [13] on the existence of a long-range statistical dependence in a chaotic process. So the variance of a FBM process verifies the following:

$$\mathrm{Var}[X(t_2) - X(t_1)] \propto |t_2 - t_1|^{2H}, \tag{9}$$

with $H \in [0,1]$. The relation between the variance and Δt [cf. Eq. (10)] is known as the diffusion function. One can make an estimate of the Hurst coefficient employing the following equation:

$$F_D(\zeta) = E\{|X(t + \Delta t) - X(t)|^2\} \propto |\Delta t|^{2H}, \tag{10}$$

where $E\{\ \}$ stands for the mathematical expectation. In the log scale, the Hurst coefficient can be easily estimated from the slope of the plot of the graphical representation of the diffusion function in the log scale:

$$\log F_D(\Delta t) = K + 2H \log|\Delta t|. \tag{11}$$

More detailed description on the diffusion function are given by Chiari *et al.* [14]. Now, the model of the FBM can be extended to the two-dimensional case and the specific of modeling the diffusion function can be undertaken, in case of the speckle pattern for the extraction of stochastic parameters, necessary for the classification of the speckle.

C. Random walk approach to spatial patterns of speckle intensity

Our starting point is the temporal relation of Eq. (10). Our objective is to apply this fractal formalism to our speckle images. To this end, we interpret spatial coordinates as time coordinates. Let r denote the position on a stripe of a speckle image and $X(r)$ the speckle intensity. Then, we replace temporal parameters by spatial parameters: $X(t)$ to $X(r)$ and $X(t+\Delta t) - X(t)$ to $u(\Delta r) = X(r+\Delta r) - X(r)$. Figure 3 shows the distribution $P(u, \Delta r)$ for several distances Δr. Furthermore, Eqs. (10) and (11) become

$$F_D(\Delta r) = E\{|X(r + \Delta r) - X(r)|^2\} \propto |\Delta r|^{2H}$$

$$\log F_D(\Delta r) = K + 2H \log|\Delta r|. \tag{12}$$

D. Extension of the FBM in two dimensions

In order to extent our analysis in two dimensions (2D), we describe speckle patterns by the coordinates x and y and generalize Eq. (12) to

$$F_{Dx}(\Delta x) = E\{|X(x + \Delta x) - X(x)|^2\} \propto |\Delta x|^{2H_x},$$

$$F_{Dy}(\Delta y) = E\{|X(y + \Delta y) - X(y)|^2\} \propto |\Delta y|^{2H_y}. \tag{13}$$

This replacement is possible because the images are considered row by row and column by column and it can therefore be assumed that the observed image is globally symmetric. However, our proposed model is not valid when the dispersion of measurements is too high, because we use the average of these measurements. Fortunately, the symmetry of the speckle for our application depends on experimental conditions. Further work in future will present this treatment in

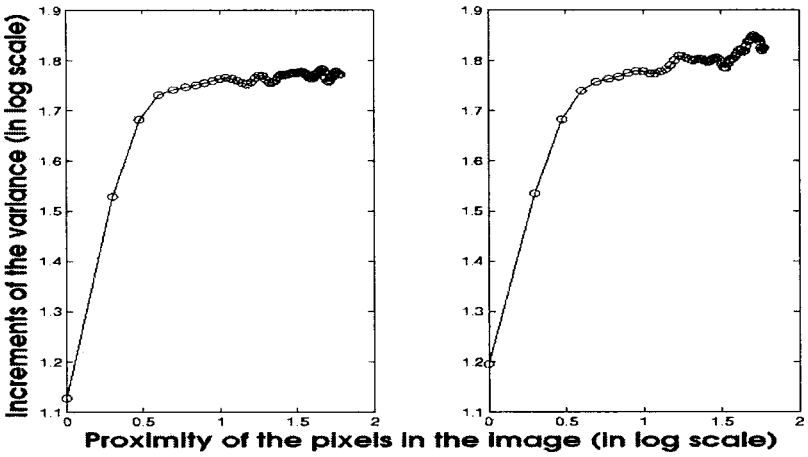

FIG. 4. Log-log graphical representation (arbitrary unity) of the speckle diffusion function of the speckle pattern shown in Fig. 1 (in both x and y directions, respectively).

polar coordinates and will aim at solving this problem. From another point of view, we can see later that this treatment makes it possible to verify isotropy in the speckle image. Let us consider an example for easy understanding of the proposed model. Let us first apply Eq. (13) to the image acquired in Fig. 1.

The results obtained for this example under consideration are shown, in log-log scale in Fig. 4. These results correspond to

$$\log F_D(\Delta x) = K_x + 2H_x \log|\Delta x|,$$

$$\log F_D(\Delta y) = K_y + 2H_y \log|\Delta y|. \tag{14}$$

Before we discuss the method employed to extract parameters from these curves, they can be systematically analyzed. These curves represent the evolution (in log scale) of the variance as function of pixels in the image. It may be noted too that the frequency-based approach may be recovered employing this notion of neighborhood on the x axis. Each curve can be considered to be composed of two parts: a "linear part," in which the average variance seems to increase linearly in the range of relatively small scales, and a so-called "saturation part," in which the variance is nearly constant. An observation of Fig. 4 and its mathematical expressions [Eq. (14)] will reveal that H_x and H_y can be easily determined from the slope of the curves in the linear part. Due to this linear property, this portion of the curve indicates the self-similarity property of the observed process, the saturation value of the average variance, and the critical scale at which the saturation appears. These parts of the curves are the most interesting ones for characterization of the fractal. Once the significance of the curves is explained, the explanations for the extraction of the parameters are presented next.

E. Adaptation of the FBM model to the speckle

The application of a fractal model to a real phenomenon needs a suitable adaptation. In the particular case of the speckle, it has been shown in Sec. II B that the experimental speckle undergoes a linear decrease in its power spectral density for high frequencies. This fact confirms that the speckle presents the property of the autosimilarity, only for the high frequencies. So, from the fractal theory [15], we can affirm that this process undergoes an autocorrelation function of the type

$$C_{ff} = \sigma^2 \exp(-\lambda|\Delta x|^{2H}), \tag{15}$$

with σ^2 the variance of the process. This enables us to explicitly determine the form of the equation of diffusion. We start from Eq. (13):

$$E\{|X(x+\Delta x) - X(x)|^2\} = 2\langle X^2(x)\rangle - 2C_{ff}. \tag{16}$$

So, after centering the process, we obtain

$$E\{|X(x+\Delta x) - X(x)|^2\} = 2\sigma^2(1 - \exp - \lambda|\Delta x|^{2H}). \tag{17}$$

This form of the equation of diffusion represents the final form of this fractal model. Here, one can draw an analogy with the theoretical-physics-based approaches used for these diffusion curves introduced by Franck *et al.* [16]. Thus, Fokker-Planck theory shows that we can express a nonlinear model as

$$F_{Dx}(\Delta x) = G_x[1 - \exp(-\lambda_x|\Delta x|^{2H_x})],$$

$$F_{Dy}(\Delta y) = G_y[1 - \exp(-\lambda_y|\Delta y|^{2H_y})]. \tag{18}$$

Three parameters provide excellent precision as demonstrated in Fig. 5. From this formulation, we obtain the saturation of the variance (G_x and G_y equal to $2\sigma^2$). The corresponding characteristic size of the speckle structure can be evaluated too, using λ_x and λ_y [cf. Eq. (19)], as found by Fournier [17]:

$$S_x = \frac{\pi}{\lambda_x},$$

$$S_y = \frac{\pi}{\lambda_y}. \tag{19}$$

Once these formulations are properly carried out, it is also possible to determine at the Hurst coefficient. It can be easily shown that, for $\Delta x \ll S_x$ and $H_x > 0.5$, Eq. (18) becomes

$$F_{Dx}(\Delta x) \propto |\Delta x|^{2H_x} \tag{20}$$

and similarly we can determine for F_{D_y}.

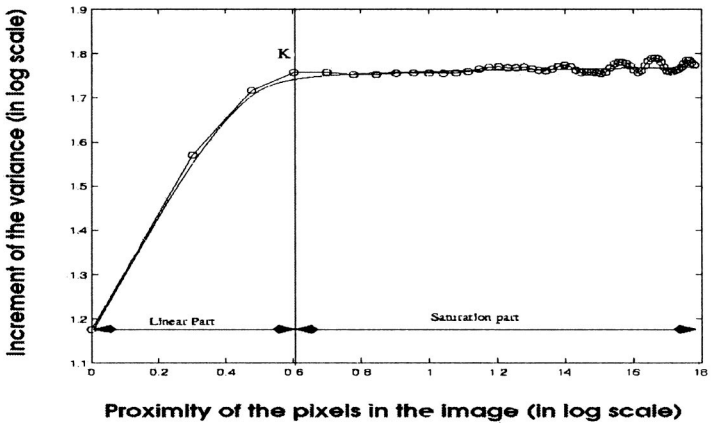

FIG. 5. Regression of the diffusion function (in the x direction) with the nonlinear model (same medium as data presented in Fig. 1).

Finally, three stochastic parameters are needed to completely characterize the speckle pattern: H, the Hurst parameter; G (or Var), which represents the saturation of the variance; and S, the characteristic size of the autosimilar element in the image.

IV. EXPERIMENTAL SETUP

Figure 6 presents our experimental setup. It is comprised of the following.

(i) A nonpolarized laser He-Ne (632.8 nm) with approximately 5 mW of power. This wavelength corresponds approximately to the maximum transparency of biological tissues.

(ii) A scattering medium composed of a solution of latex balls.

(iii) A Texas Instrument TC-255 charge-coupled-device (CCD) camera with 336×244 pixels. The sensor has the following characteristics: each pixel measures 10×10 μm, its capacity is about 62 500 electrons, and its dynamics is 66 dB. The sensitivity of the camera is 5×10^{-4} lux and exposure time for capturing the speckle was 10 ms for our acquisition.

(iv) In our work the EDITIM+ software was employed, which is equipped with many image processing capabilities—e.g., correction of the thermal noise by subtracting a "black" image to each acquisition.

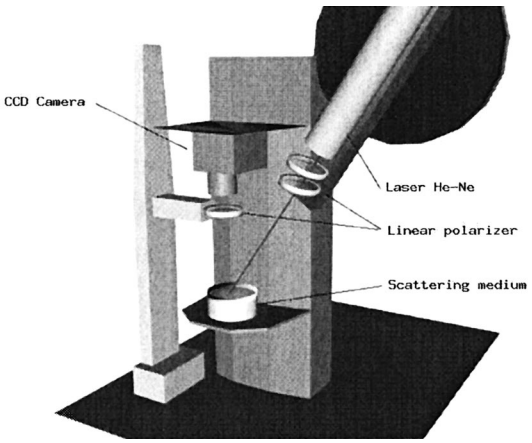

FIG. 6. Experimental setup.

(v) Two linear polarizers at the input/output of the device.

The accuracy of the measurement is maximized by the simplicity of this device. The CCD sensor is directly exposed to the backscattered radiation, without using a lens. The exposure time is set to 10 ms. The sample-sensor distance (30 cm) is maintained constant for all acquisitions. Theoretically, the minimum speckle size for this distance is about 50 μm. This distance was optimized so we could acquire several pixels per speckle grain and retain the global statistics of the speckle. Thus, each speckle of our media is recorded under identical conditions. A detailed description of the experimental setup is given now.

Linear polarizers were placed at the input/output of the device. Our acquisitions were all performed with two configurations of these polarizers. The incident light was linearly polarized. According to Bicout and Brosseau [18], one can observe an exponential loss of polarization following diffusion events. Hence, the photons that originate from the bulk after diffusion are statistically more depolarized than the photons that originate from the surface of the observed medium. Thus, when the output polarizer is placed perpendicularly to the input one, we have the privilege of observing the speckle which originates from the volume. Conversely, when both polarizers are parallel, we can observe the surface speckle.

In the next section, we present the application on our test media.

V. RESULTS

In our work, we have considered the test media as solutions of 812-nm- (with standard deviation of 0.015 μm) diameter latex balls with several concentrations. This diameter corresponds to the size of the main diffusers of human skin. The concentrations are kept at 1%, 5%, and 10% in those balls. The speckle is captured using both the configurations of the input/output polarizers. For each configuration, 20 acquisitions were undertaken. Then, we compare the mean parameters, which depend on the x and y directions, the concentration in latex balls, and the position of the polarizers. The results obtained from an analysis of the variance enables us to discuss the significance p of the measurements. Examples of the speckles to be characterized are shown in Fig.

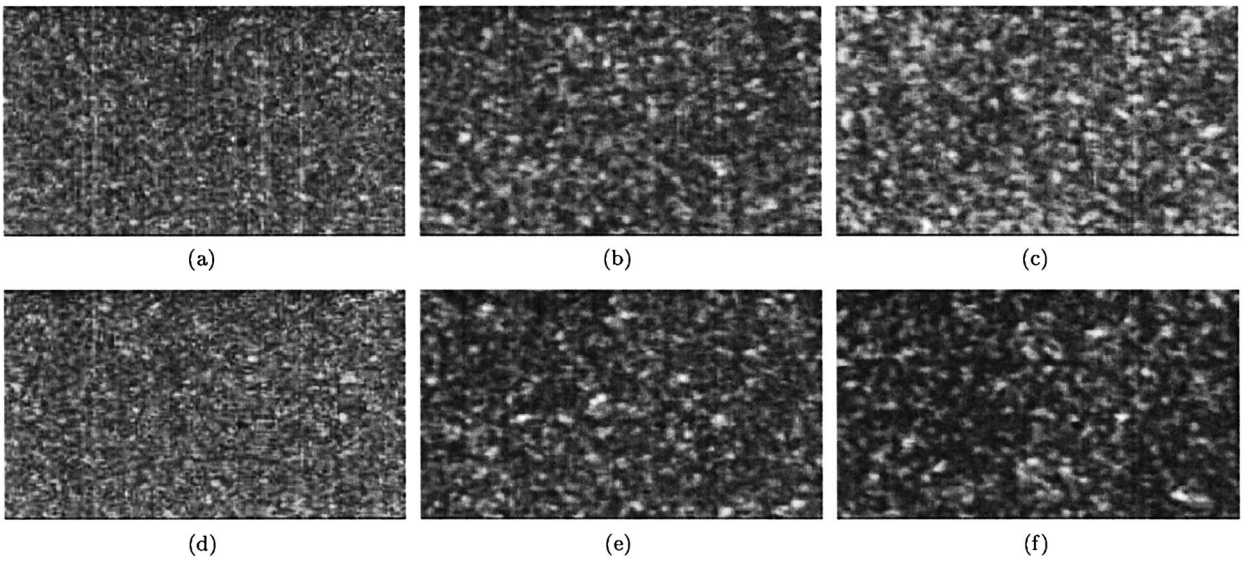

FIG. 7. The speckles of several media.

7. The first row shows the speckles for the three concentrations (1%, 5%, and 10%, respectively) with the polarizers in perpendicular configuration. The second row corresponds to the parallel configuration of the polarizers.

A. Fokker-Planck model

The results obtained with the model are shown in Fig. 8 and are summarized in Table I.

1. Evolution of the first parameter: Hurst coefficient H

This parameter is not significant for each configuration ($p > 0.05$). Furthermore, this cannot be utilized to characterize the speckle in this application. This can be explained by the fact that in this continuous model, H represents the Hurst coefficient at small scales. Only high frequencies contribute to its value. It therefore seems interesting to note the constant

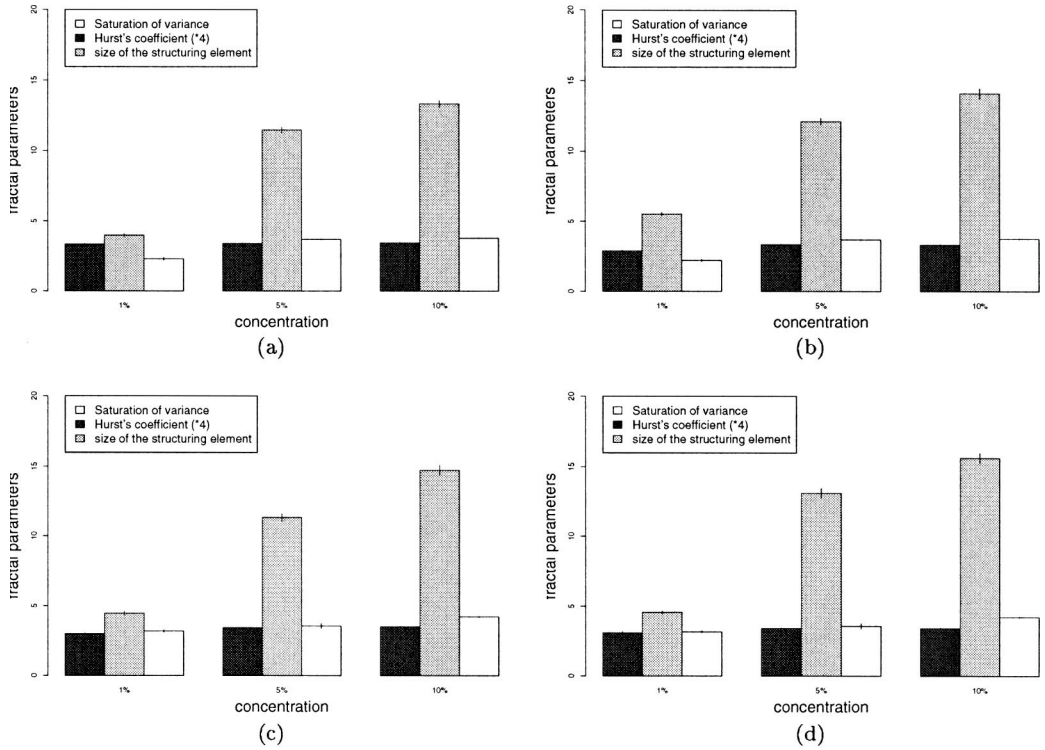

FIG. 8. The evolution of the fractal parameters according to concentration. (a) Perpendicular configuration of polarizers in the x direction, (b) perpendicular configuration of polarizers in the y direction, (c) parallel configuration of polarizers in the x direction, and (d) parallel configuration of polarizers in the y direction.

TABLE I. Results of the Fokker-Planck model.

Configuration	Concentration 1%				Concentration 5%				Concentration 10%			
	⊥		∥		⊥		∥		⊥		∥	
Direction	*x*	*y*	*x*	*y*	*x*	*y*	*x*	*y*	*x*	*y*	*x*	*y*
Variance	2.30	2.21	3.18	3.15	3.68	3.68	3.55	3.56	3.77	3.73	4.21	4.21
(*G*)	±0.18	±0.17	±0.16	±0.15	±0.06	±0.08	±0.35	±0.39	±0.05	±0.07	±0.06	±0.08
Characteristic size	3.97	5.51	4.47	4.57	11.48	12.10	11.32	13.07	13.33	14.08	14.72	15.60
(pixels)	±0.25	±0.27	±0.25	±0.18	±0.38	±0.48	±0.50	±0.70	±0.47	±0.70	±0.71	±0.70
Hurst's coefficients	0.83	0.72	0.75	0.77	0.85	0.83	0.85	0.85	0.86	0.83	0.87	0.85
(*H*)	±0.02	±0.02	±0.02	±0.04	±0.02	±0.02	±0.02	±0.02	±0.02	±0.02	±0.02	±0.02

nature of the fractal dimension of the speckle when only high frequencies are considered.

2. Evolution of the second parameter: Saturation of variance Var

One can foresee the saturation of this parameter with concentration. The *X* and *Y* directions present nearly the same results for all configurations. When the input/output polarizers are parallel, this parameter gives a significant characterization of the various concentrations ($p<0.0001$). In the perpendicular configuration of the polarizers, the difference between 5% and 10% concentration is not significant ($p>0.05$). It is interesting to note that, for each concentration, we may observe differences ($p<0.01$) between parallel and perpendicular configurations of the polarizers.

3. Evolution of the third parameter: Size of the characteristic elements S

This parameter presents significant difference between the concentrations in all the configurations ($p<0.01$) except for 5% concentration where differences between perpendicular and parallel polarizer configurations are not significant ($p>0.05$). It was also noted that differences between *X* and *Y* directions are not significant ($p>0.05$) for 1% concentration in the parallel configuration of the polarizers.

A detailed discussion on our results should be useful to clarify the usefulness and limits of our model.

B. Discussion

The proposed model showed interesting results.

When applied to our test media, the model does not show any significant difference for different configurations of the polarizers. As explained earlier, polarization is used to filter the speckle. In the perpendicular configuration of the polarizers, we observe the speckle that originates from the bulk, opposed to the speckle which originates from the surface, observed in the parallel configuration of the polarizers. No significant difference could be observed between these configurations and we could not, therefore, discriminate surface speckle from volume speckle. This can be explained from the fact that our test media had only one phase. Further work in the future will be devoted to the discrimination between surface and volume speckles in a multilayer medium. The three models showed no great difference between *X* and *Y* directions either. Only a little anisotropy in our measurement could be observed due to the symmetry of the experimental setup employed.

Our next discussion encompasses our main research interest described in this paper—i.e., the evolution of the fractal parameters with the concentration of the media. We observed an increase of the parameters with the concentration of latex balls in the test media. However, we could also foresee a saturation phenomenon of the discrimination with the concentration. It seems difficult to evaluate the limits of the discrimination with this fractal method. Nevertheless, the characteristic size of the structuring element appears to be the most discriminating parameter. This parameter presents a positive correlation with the concentration and increases when the concentration increases. Finally, the fractal approach can be used to discriminate the speckle obtained in backscattering.

VI. CONCLUSIONS

In this paper, we present a novel method for the study of the speckle statistics. This method, based on Brownian motion theory, is more powerful than the classical frequency-based approach, because of its multiresolution and multiscale properties. In our view, the fractal approach seems more appropriate to study a nonstationary and nonlinear phenomenon such as the speckle of a multiscattering medium. Hence, we first presented our fractal approach based on the fractional Brownian motion theory. This led us to the diffusion function, which contains the fractal information on the medium observed. Second, we implemented the model necessary for the exploitation of the diffusion function. Hence, the details of the experimental setup were presented and we applied the fractal formulation to the images obtained in backscattering from test media. The test media were composed of latex balls in solution. It could be observed that fractal parameters such as the Hurst coefficients, characteristic size of structuring element, and saturation of variance enabled us to characterize the observed medium. Further work will be carried out to determine the limits of these methods. We hope to generalize

the study of speckle patterns employing fractal theory to characterize, discriminate, or classify any scattering medium using its speckle. Fractal theory has a broad spectrum and can be used in a statistical approach, as presented in this paper, as well as in a structural approach, which we intend to present in another paper. It is sincerely hoped that useful applications will be possible in biomedical imagery and more precisely in dermatology, where several pathologies could be detected at an early stage. Indeed, many pathologies cause modifications of the optical properties of the skin, and it should therefore be possible to detect them utilizing the speckle phenomenon.

ACKNOWLEDGMENTS

We wish to thank P. Gourmelon and DPHD\IRSN Institute (Fontenay-aux-roses, France) for financial assistance during this research. S.G. also wishes to thank P. Siarry for his assistance in the correction of this paper.

[1] L.H. Enloe, Bell Syst. Tech. J. **46**, 1479 (1967).
[2] L.I. Goldfischer, J. Opt. Soc. Am. **55**, 247 (1964).
[3] Y. Piederriere, J. Cariou, Y. Guern, B. Le jeune, G. Le Brun, and J. Lotrian, Opt. Express **12**, 176 (2004).
[4] J.W. Goodman, in *Laser Speckle and Related Phenomena*, edited by J.C. Dainty (Springer-Verlag, Berlin, 1984) pp. 9–75.
[5] M. Françon, *Granularite Laser* (Masson, Paris, 1978).
[6] C.E. Halford, W.L. Gamble, and N. George, Opt. Eng. **26**, 1263 (1987).
[7] Q.B. Li and F.P. Chiang, Appl. Opt. **31**, 6287 (1992).
[8] G.P. Weigelt and B. Stoffregan, Optik (Stuttgart) **48**, 399 (1977).
[9] A.Z. Genack and J.M. Drake, Europhys. Lett. **11**, 331 (1990).
[10] M.A. Webster, K.J. Webb, and A.M. Weiner, Phys. Rev. Lett. **88**, 033902 (2002).
[11] J.W. Goodman, *Statistical Optics* (Wiley Intersciences, New York, 1985).
[12] B.B. Mandelbrot, *The Fractal Geometry of Nature* (Freeman, San Francisco, 1983).
[13] H.E. Hurst, Trans. Am. Soc. Civ. Eng. **116**, 770 (1951).
[14] L. Chiari, A. Bertani, and A. Cappello, Human Mouvement Sci. **19**, 817 (2000).
[15] P. Abry, P. Gonçalves, and P. Flandrin, in *Spectrum Analysis and* $1/f$ *Processes*, edited by A. Antoniadis and G. Oppenheim (Springer, Berlin, 1995).
[16] T.D. Franck, A. Daffertshofer, and P.J. Beek, Phys. Rev. E **63**, 011905 (2000).
[17] R. Fournier, Ph.D. thesis, University of Paris 12, 2002.
[18] D. Bicout and C. Brosseau, J. Phys. I **2**, 2047 (1992).